Atmospheric Environment Vol. 22, No. 5, pp. 839–851, 1988.
Printed in Great Britain.

0004–6981/88 $3.00 + 0.00

BOUNDARY LAYER WIND PARAMETERIZATION FOR USE IN A LAGRANGIAN TRAJECTORY MODEL

SUZANNE M. VIESSMAN and SETHU RAMAN
Department of Marine, Earth and Atmospheric Sciences, North Carolina State University, Raleigh, NC 27695-8208, U.S.A.

(*First received* 5 *May* 1986 *and received in final form* 23 *September* 1987)

Abstract—Parameterization of mean boundary layer flow over two contrasting types of terrain for unstable (day) and stable (night) atmospheric conditions is developed and incorporated in a Lagrangian trajectory puff model. Boundary layer observations, classified and analyzed through the method of least squares, provide a wind formulation which in effect reduces the wind speed and backs the wind direction relative to surface geostrophic flow. Model sensitivity to the wind modification is determined qualitatively through comparison of modified and original model trajectories to plume observations from the Cross-Appalachian Tracer Experiment (CAPTEX 83). Results indicate that in this particular application (i.e. short-term), both techniques have limitations. Modified trajectories, however, appear to more closely define the plume domain near the source, but lag the observed flow in terms of distance traveled.

Key word index: Transport model, trajectory, boundary layer, geostrophic.

1. INTRODUCTION

Long-range transport is an integral phase of the acidic deposition phenomenon. Motivation for research in this area stems from the need to identify source–receptor relationships on the regional scale. Numerous models have been developed to address this task. Each model presents a particular solution to the transport problem while reflecting the inevitable compromise between accuracy and economy that attends modeling endeavors (Johnson, 1983). Lagrangian trajectory models characteristically define source–receptor relationships at a reasonable level of computational efficiency (Johnson, 1983). Such an attribute is essential to the use of models on an operational basis.

This paper describes boundary layer wind parameterization for use in a Lagrangian trajectory puff model. Boundary layer observations are classified and analyzed through the method of least squares to provide an expression for mean boundary layer flow over two different types of terrain for unstable (day) and stable (night) atmospheric conditions. Trajectories are produced from modified and original versions of the model and compared with observations from the Cross-Appalachian Tracer Experiment (CAPTEX 83; Ferber *et al.*, 1986) to indicate, in a qualitative sense, the response of the model to the adjustments proposed.

2. SURFACE GEOSTROPHIC FLOW AS AN APPROXIMATION OF ACTUAL FLOW

As is well known, the geostrophic wind is the expression of large-scale flow in the atmosphere. The direction of the geostrophic wind is indicated by the orientation of the isobars and the speed by their lateral spacing (Hess, 1979). One of the reasons for using the surface geostrophic wind in transport modeling is revealed through a comparison of the spatial and temporal resolutions of the observational networks. The surface observational network has a spatial resolution of approximately 100 km and a temporal resolution of 1 h (Rao *et al.*, 1983). In comparison, wind fields at other pressure levels are constructed from a network with a spatial resolution of 300–400 km and a temporal resolution of 12 h. The interpolation required by the coarser space and time scales of the upper-air network potentially smooths variations out of the transport wind, thus affecting its accuracy relative to surface-based trajectories (Ellenton *et al.*, 1985; Smith and Hunt, 1978). An additional reason for utilizing the surface geostrophic wind rests in the expectation of this wind to lie within a sector defined by the surface and upper-level wind vectors when projected onto a horizontal plane. Considering that the transport wind of a thoroughly mixed air mass should be an average of the surface and upper-level winds, the surface geostrophic wind is thus thought to provide better representation, relative to these winds (Ellenton *et al.*, 1985).

To afford the most realistic wind simulation, it is essential to capture the interaction of flow at various scales and especially the flow within the boundary layer, as it is the physics of this layer that determines the initial dispersion of pollutants, affects their transport and transformation and dictates their eventual removal. During daytime convective conditions, boundary layer winds are usually observed to be subgeostrophic and oriented down the pressure gradient.

In light of this, the surface geostrophic wind is considered a poor approximation of actual wind in the boundary layer (Clarke, 1970). Geostrophic flow by definition omits speed and curvature accelerations, which are retained with the use of observed wind data (Szepesi, 1978). Trajectory errors are likely to be unavoidable, then, in situations in which the track of the trajectory encounters an area of strong isobaric curvature, as occurs near the center of a low pressure system, or in which the air mass is strongly baroclinic (Smith and Hunt, 1978). Transport based on the surface geostrophic wind assumes a constant wind direction, parallel to the isobars. Thermal wind equations, however, indicate the tendency of wind to back with height in regions of cold air advection and veer in regions of warm air advection (Rao *et al.*, 1983).

3. MEAN BOUNDARY LAYER TRANSPORT

As mentioned previously, it is the dynamics of the boundary layer which governs the evolution of pollutants released in the atmosphere. Pollutant emission and transport principally occur within 2 km of the surface typically the extent of the boundary layer during the daytime summer months (Gillani, 1983). The height of the daytime boundary layer is significant in that it defines the maximum depth through which pollutants are mixed during a diurnal cycle (Fisher, 1984). The atmospheric residence time of tall stack emissions, a critical factor in estimating the impact of pollutants, may vary substantially due to the seasonal difference in this height.

Determination of a representative daytime transport wind is fairly straightforward assuming typical profiles of the convective boundary layer. In the sense that wind speed and potential temperature are constant throughout the boundary layer depth, the daytime layer is regarded well-mixed and this characteristic is likewise attributed to pollutants within the layer (Thorpe and Guymer, 1977). This is not an unreasonable assumption for an unstable atmosphere, which is typified by strong buoyant and mechanical mixing. Under such atmospheric conditions, a single-layer average wind is commonly used to represent boundary layer transport.

During the night, over land with clear sky, identification of an appropriate transport wind is complicated by the highly stratified nature of the nocturnal atmosphere. In early evening, rapid cooling of the surface and adjacent air leads to the development of a stable boundary layer exhibiting large gradients and strong shears of wind speed and direction. Near the surface a shallow turbulent depth of the order of tens of meters often exists in which material may be somewhat mixed. The inversion layer commonly extends to a greater height, usually less than 300 m (Hoxit, 1974). The phenomenon of an accelerated low-level wind is associated with nocturnal stable conditions. Pollutants released from stacks above this level of maximum wind speed typically demonstrate minimal diffusion and tend to be transported with the air aloft. These characteristics combine to inhibit simple definition of a nocturnal transport wind.

Mixed-layer trajectory models employ a single-layer average wind as the transport wind. While the concept of modeling a single layer with constant mean quantities may be justified for an unstable (daytime) atmosphere (Thorpe and Guymer, 1977), it is emphasized that such a model will only reflect true conditions if the boundary layer is, in actuality, well-mixed and without the affect of shear (Samson, 1980). Anthes *et al.* (1980) compared the performance of a one-dimensional mixed-layer model with that of a two-dimensional multi-level model. Under horizontally homogeneous conditions, mean values of the velocity components were in close agreement. With the introduction of inhomogeneity and complex terrain, however, relative limitations of the mixed-layer model in the prediction of boundary layer flow became evident.

Given the assumption of a well-mixed, daytime boundary layer over land, a mean boundary layer wind may be regarded as a valid expression of transport within the layer. Employing a single layer average wind as the transport wind under nocturnal conditions must be considered a most rough approximation. Reasoning for adopting this approach stems from the interest in maintaining a simplified transport model, implying use of single-layer average winds. Candidates for the uppermost limit of integration in the determination of a layer average wind are the nocturnal boundary layer (NBL) height and the elevated inversion height (i.e. remnant of the previous day's boundary layer height). Data from the Sulfate Regional Experiment (Hidy, 1984) indicate that for the summer and winter seasons most SO_2 emissions enter the atmosphere above 100 m. This level is of the order of the nocturnal boundary layer height. As a means of incorporating all levels of pollutant transport and emission, the elevated inversion height is selected as the upper limit of the nocturnal transport layer.

4. BASIS OF WIND PARAMETERIZATION

To quantify the relationship between the mean boundary layer and surface geostrophic wind, regressions based on the following models are performed:

$$\bar{U} = bG \tag{1}$$

$$\bar{V} = b'G \tag{2}$$

where $\bar{U}$ and $\bar{V}$ are mean boundary layer wind components, with $\bar{U}$ aligned parallel to the surface geostrophic wind; G is the magnitude of the surface geostrophic wind vector; and b and b' are regression coefficients. While empirical, the relationships thus obtained avoid a coordinate system dependency and allow for expressions of geostrophic speed and directional change for model application.

4.1. *Data selection*

Data used in the regressions are from the Wangara (34° 30′ S, 144° 56′ E; Clarke *et al.*, 1971) and Koorin Expeditions (16° 16′ S, 133° 23′ E; Clarke and Brook, 1979). These databases provide the most extensive compilations of the required information. To obtain a congruous set of observations, day and night soundings are chosen so as to most closely reflect a barotropic atmosphere. Specifically, data are omitted for the conditions given below, following criteria presented by Arya (1975) for the determination of similarity functions:

(1) rain, haze or dust devils reported at the time of sounding

(2) occurrence of a frontal passage within approximately 6 h of the sounding time

(3) incomplete data (also soundings highlighted as 'faulty pressure' or 'humidity very high or low', since such designation is thought to introduce error into the determination of the boundary layer height)

(4) indeterminate inversion height.

Synoptic charts accompany the Wangara data, facilitating determination of a frontal passage, whereas periods of excessive cloud are avoided with the Koorin data. Hours designated for analysis are 1200 and 1500 LT for the daytime cases and 2100, 0000 and 0300 LT for the night-time cases. Day soundings are assumed representative of fully-developed boundary layers, while night soundings are selected so as to avoid transitional periods. Data are partitioned into clear day and clear night sets for each wind component. 'Clear' observation times are defined as those for which the reported sky cover is $\leqslant 1/8$. Regression data sets are further classified according to surface roughness, as the Wangara and Koorin data represent distinct roughness lengths (z_0). For convenience, Wangara regression sets are labeled as 'smooth' (average $z_0 = 0.004$ m), and those of the Koorin sets as 'rough' (average $z_0 = 0.65$ m; Garratt *et al.*, 1982).

Wind profiles from the Wangara data reflect a five-station, mesoscale average, while those from the Koorin set are from double theodolite observations. Surface geostrophic winds used in the analysis of the Wangara data are representative of the larger, 19-station barometer network, reported 3-hourly. For the Koorin observations surface geostrophic winds are determined from a five-station barometer network established on a roughly 150 km grid (Clarke and Brook, 1979).

The daytime boundary layer height is identified as the height of the lowest significant inversion, while the elevated inversion height (i.e. remnant of the previous day's boundary layer height) distinguishes the upper limit of the nocturnal transport layer. Wangara boundary layer heights are determined from virtual potential temperature profiles. Inversion heights for the Koorin cases are determined from the temperature soundings provided, given the absence of accompanying humidity profiles.

Mean boundary layer wind components are obtained for each of the chosen soundings via integration of the u and v profiles. Each profile is integrated separately, according to Simpson's Rule if the number of intervals involved in the integration is even and according to the trapezoidal rule if the number of intervals used is odd. For boundary layer heights above 1000 m, the interval is taken to be 100 m (data are reported in 50 m intervals below 1000 m and in 100 m intervals above this level). As the equations of motion strictly apply to the boundary layer, the mean wind components used in the night-time regressions are not obtained from a single integration, but are produced by summing the integrated values of the lower (surface to NBL height) and upper (NBL height to elevated inversion height) layers and dividing through by the maximum boundary layer depth. The nocturnal boundary layer height for both the Wangara and Koorin sets is identified as the height of the low-level wind maximum (determined from wind speed profiles).

For a number of individual observations, the vector relationship between the surface geostrophic, surface and mean boundary layer winds is not as expected for a barotropic atmosphere (i.e. in the southern hemisphere the surface and/or mean boundary layer winds are not veered with respect to the geostrophic, or the mean boundary layer wind is found to lie outside the sector defined by the surface and geostrophic winds). In the Koorin data sets this is principally a matter of the surface wind not being veered with respect to the mean boundary layer wind. With the Wangara data sets it is more a matter of the mean boundary layer wind not being veered with respect to the surface geostrophic wind. In the night-time case such occurrences are understandable as the mean boundary layer wind components used are those representative of the layer defined by the surface and elevated inversion height and hence do not strictly reflect boundary layer properties. Unusual vector relationships expressed in the daytime regression sets are thought to reflect the occurrence in the boundary layer of cold and/or warm air advection, which violates the underlying assumption of a barotropic atmosphere. For comparison, regressions are also run on subsets of the original data sets in which these anomalous observations have been removed. Since absolute values of the wind components are used, anomalous and conventional observations are treated the same in the original data set regressions (see Appendix for the listing of values employed). In essence, these regression sets involve all relationships of the mean boundary layer wind components and the surface geostrophic wind vector for the observations selected. After deletion of the anomalous occurrences from the Wangara original day set only two observations are found to remain. To allow for comparison, ratios of the boundary layer components to the respective surface geostrophic component are averaged between the two observations to yield the necessary coefficients.

Table 1. Sets of regression coefficients and vector relationships obtained by regressing mean boundary layer wind components on the surface geostrophic wind†

Original sets	Number of observations	Subsets	Number of observations
Wangara day $\bar{U} = 0.73G$ $\bar{V} = 0.17G$ $MW = 0.75G$ Backing angle = 13°	8	Wangara day $\bar{U} = 0.72G$* $\bar{V} = 0.14G$* $MW = 0.73G$* Backing angle = 11°*	2
Wangara night $\bar{U} = 1.08G$ $\bar{V} = 0.16G$ $MW = 1.09G$ Backing angle = 8°	28	Wangara night $\bar{U} = 1.12G$ $\bar{V} = 0.15G$ $MW = 1.13G$ Backing angle = 8°	16
Koorin day $\bar{U} = 0.39G$ $\bar{V} = 0.21G$ $MW = 0.44G$ Backing angle = 28°	10	Koorin day $\bar{U} = 0.32G$ $\bar{V} = 0.30G$ $MW = 0.44G$ Backing angle = 43°	5
Koorin night $\bar{U} = 0.50G$ $\bar{V} = 0.40G$ $MW = 0.64G$ Backing angle = 39°	8	Koorin night $\bar{U} = 0.52G$ $\bar{V} = 0.43G$ $MW = 0.67G$ Backing angle = 39°	6

* Values represent the average of two observations.

† Here G is the magnitude of the surface geostrophic wind vector and MW signifies the magnitude of the mean boundary layer wind vector.

4.2. *Statistical analysis and results*

Results of the regressions involving the surface geostrophic wind vector as the independent variable are shown in Table 1. Speed and directional change of the geostrophic wind are determined from the component expressions and are identified for each regression set. Confidence intervals for the regression coefficients are provided in the Appendix. Relative coefficients obtained from the original and subset regressions appear similar in magnitude, with the greatest distinction occurring between the Koorin day sets, in which the backing angles produced vary by 15 degrees.

It is of interest to determine whether or not the derived vector relationships are physically realistic. Observations indicate that the magnitude of the cross-isobar (backing) angle increases with increasing surface roughness, increasing stability and decreasing latitude (Haltiner and Martin, 1957). Although the increase of backing angle with surface roughness and latitude cannot be independently determined, given both the greater surface roughness and lower latitude of the Koorin data sets, the relative magnitudes of the backing angles of the Wangara and Koorin sets are according to expectation. Comparison between stable and unstable conditions is inappropriate given the definition of the mean boundary layer wind for the night-time case. As anticipated, a greater reduction of the surface geostrophic wind speed is demonstrated by the Koorin (rough) regression sets. The amplification of the coefficients at night likely involves the inclusion of the low-level wind speed maximum in the derivation of the layer average wind. Relatively smaller coefficients associated with the V components may be attributed to the general greater magnitude of the U component for all data sets. In essence, the coefficients obtained relate to the general nature of the boundary layer wind to be backed and reduced in speed with respect to the geostrophic wind (northern hemisphere).

In light of the overall similarity between the regression results of the original and subset data, it was decided to utilize the results of the original sets, as the more numerous observations associated with these sets lend greater statistical significance to the proposed (least squares) fits. Consequently, the following discussion is limited to the regressions involving the original data sets.

Results of the original Wangara daytime regressions indicate use of the model $\bar{U} = bG$ (where b is the regression coefficient) for the U component run. Neither the intercept nor the geostrophic term are found to be significant with the V component run. Wangara night-time regressions indicate significance of the intercept and geostrophic terms for both U and V component runs.

Koorin daytime regressions suggest use of the reduced model for the U component. Comparison of residual plots indicates that a better fit is achieved with retention of the intercept for the V component case. Results of the Koorin night-time regressions support the use of the reduced model for the U component case; no terms are found significant for the V component.

Table 2. Statistics corresponding to regressions of the mean boundary layer wind components on the magnitude of the surface geostrophic wind (G), including an intercept (INT)*

			U Component				V Component			
		n	EST	SE	p	R^2	EST	SE	p	R^2
Wangara day	G	8	0.987	0.195	0.002	0.811	0.078	0.222	0.737	0.020
	INT		−2.161	1.624	0.232		0.744	1.854	0.702	
Wangara night	G	28	0.774	0.149	0.000	0.510	−0.212	0.100	0.008	0.146
	INT		2.600	1.244	0.047		3.159	0.839	0.000	
Koorin day	G	10	0.638	0.124	0.000	0.768	−0.337	0.096	0.008	0.607
	INT		−2.762	1.321	0.070		6.021	1.021	0.000	
Koorin night	G	8	0.709	0.150	0.003	0.788	0.034	0.196	0.866	0.005
	INT		−1.940	1.338	0.197		3.363	1.748	0.103	

* Here EST represents the parameter estimate, SE and p are the associated standard error and significance probability value and n is the number of observations. All values pertain to regressions of the original data sets.

Table 3. Statistics corresponding to regressions of the mean boundary layer wind components on the magnitude of the surface geostrophic wind (G), without an intercept*

			U Component			V Component		
		n	EST	SE	p	EST	SE	p
Wangara day	G	8	0.733	0.038	0.000	0.166	0.039	0.004
Wangara night	G	28	1.077	0.037	0.000	0.156	0.029	0.000
Koorin day	G	10	0.388	0.039	0.000	0.208	0.055	0.004
Koorin night	G	8	0.496	0.033	0.000	0.404	0.047	0.000

* Here EST represents the parameter estimate and SE and p are the associated standard error and significance probability value, respectively. All values pertain to regressions of the original data sets.

Table 2 shows the regression coefficients with their associated standard errors and p values for regression of the mean boundary layer wind components on the magnitude of the surface geostrophic wind, including an intercept. Values of R^2 (square of the correlation coefficient) for the respective regressions are also included. Understanding that p represents the lowest significance level at which the null hypothesis could be rejected with the data, the smaller the p value, the stronger the evidence for rejecting the null hypothesis. Here the null hypothesis is that the parameter estimate (i.e. the slope or intercept) is equal to zero. One can see that the greatest percentages of the variance explained by the regression model are associated with the Wangara day and Koorin day and night U component sets. The least significant fits are associated with the V component regressions. Statistics relevant to the no-intercept regressions are provided in Table 3.

Values of R^2 for the no-intercept model are not comparable to those of the intercept model and are therefore not included. (With the intercept model R^2 stands for the proportion of the variation around the mean of the dependent variable which is accounted for by the regression. Values of R^2 in the no-intercept model, however, signify the proportion of the variation around the origin which is accounted for by the regression.)

To determine whether or not the regression coefficients obtained are statistically different, values of t are computed using the formula:

$$t = (b_1 - b_2)/(SE_1^2 + SE_2^2)^{1/2}$$

where b_1 is the regression coefficient and SE_1 its standard error from the first sample and similarly b_2 and SE_2 for the second sample. Unequal variances are assumed and the degrees of freedom are found as: $n_1 + n_2 - 2$, where n is the sample size (degrees of freedom were also computed using Welch's approximation; their associated critical t values do not change the outcome of the hypothesis tests). These statistics are presented in Table 4. Inspection of the p values reveals three cases in which the coefficients are not found to be statistically different. These cases all involve the V

Table 4. Values of the student's t statistic and significance probability value (p) for testing the hypothesis that the population regression coefficients are equal for the regression pairs indicated*

	U Component		V Component	
	t	p	t	p
Wangara day / Wangara night	−6.428	0.000	0.209	0.835
Wangara day / Koorin day	6.345	0.000	−0.631	0.538
Wangara day / Koorin night	4.676	0.000	−3.894	0.002
Wangara night / Koorin day	12.853	0.000	−0.846	0.403
Wangara night / Koorin night	11.664	0.000	−4.491	0.000
Koorin day / Koorin night	−2.137	0.048	−2.690	0.016

* Here all regression pairs pertain to the no-intercept model.

component and are the Wangara day and night, the Wangara and Koorin day and the Wangara night and Koorin day regressions. This outcome is not surprising given the close magnitudes of the respective coefficients. The p value for the Koorin day and night U component regressions is just slightly less than the critical value of 0.05, indicating marginal rejection of the null hypothesis.

5. APPLICATION OF WIND PARAMETERIZATION

5.1. *Model description*

The sets of geostrophic wind adjustments are applied to a Lagrangian trajectory puff model developed by the Air Resources Branch of the Ontario Ministry of Environment (Ellenton *et al.*, 1985). Model operation occurs on a 37 by 38 subset of the Canadian Meteorological Center (CMC) grid, centered on the Great Lakes. Grid increments are 127 km. Under the existing formulation, winds are derived from a smoothly varying pressure field which is obtained by the fitting of ninth degree orthogonal polynomials to observed pressure data. Continuous point source emissions are modeled as discrete puffs travelling along trajectories defined by a variable surface geostrophic wind field. As the pollutant mass is transported it undergoes chemical transformation and is subject to both wet and dry deposition.

5.2. *Computation of trajectory endpoints*

The model employs an iterative approach to determining trajectory endpoints. Initially no acceleration of the wind is assumed and the first guess at the next trajectory endpoint X_1 is given by:

$$X_1 = X_0 + U_0 \Delta t$$

where X_0 is the trajectory starting point, U_0 is the corresponding geostrophic velocity and Δt is the prescribed time step. In the revised model U_0 is modified to reflect the influence of surface type (rough or smooth) and stability (day or night condition) pertinent to the starting location X_0 (the basis of incorporating these influences is explained in later sections). This initial guess trajectory endpoint is regarded as an indicator of the likely change in surface type encountered during the particular time step. If the surface type associated with the current location of the endpoint differs from that of the starting point, it is inferred that the path of the wind during the given time step involves a change in surface type. To incorporate this change, a second guess trajectory endpoint is calculated as:

$$X_2 = X_0 + (U_0 + U_1)/2\Delta t$$

where U_1 is the geostrophic velocity associated with the initial guess point X_1 above and the averaged velocity is modified according to the surface type and stability at X_1. Provided U_0 and U_1 are not equal, an acceleration of the wind is now realized as $(U_1 - U_0)/\Delta t$. A third guess at the next trajectory endpoint is made by replacing U_1 with U_2, the geostrophic velocity corresponding to X_2 and modifying the average velocity according to conditions at X_2:

$$X_3 = X_0 + (U_0 + U_2)/2\Delta t.$$

At this point the endpoints X_2 and X_3 are compared and if found to be within the convergence limits (approximately equal to 10% of the normalized grid), then the new trajectory endpoint is designated as X_3. If the points violate the convergence criterion, then another guess is made, replacing U_2 with U_3 in the above equation to yield X_4. The points X_4 and X_3 are compared and the series of calculations and checks continues until the convergence criterion is met.

5.3. *Incorporation of surface roughness*

As an initial means of incorporating the change of wind with surface roughness, squares of the CMC grid are assigned a landuse type of zero (rough) or one (smooth) depending upon whether or not the greater percentage of area in that square is classified as land or water. The land/water classification is realized through adaptation of a landuse data base developed by the National Center for Atmospheric Research (NCAR). This data base extends from 67 to 105 degrees longitude and from 24 to 50 degrees latitude. The total area is described by a matrix of 152 by 156 grid cells, given 1/4 degree longitude and 1/6 degree latitude increments, respectively. Per grid cell, the data base supplies the percentage of grid area relating to each of nine landuse categories. This information is converted to the CMC grid, at which point the percentages of all non-water landuse types are summed and compared to the percentage of water represented to yield an overall landuse designation for each grid square. The surface type assigned at each trajectory endpoint is the surface type corresponding to the CMC grid square in which that point resides.

It is acknowledged that depending upon the thermal characteristics of a given water surface, stability over the water may also be an issue and may have a different effect relative to that over land. Since surface temperatures of large bodies of water do not generally have significant diurnal variation, the over-water atmospheric stability will greatly depend on the air–water temperature difference. In this study only surface distinction in terms of roughness is approximated.

The decision to avoid any distinction between non-water surfaces stems from the dual nature of the wind modification scheme. The smooth set of coefficients correspond to a roughness length of 0.004 m (average z_0 determined from the Wangara observations) which is more of the order of z_0 associated with a water surface ($0.1–10.0 \times 10^{-5}$ m; Oke, 1978). In contrast, the rough set of coefficients represents a roughness length of 0.65 m (average z_0 of the Koorin observations) which falls within the general range of roughness lengths defined by non-water surfaces (0.05–1.0 m; Sheih *et al.*, 1979). At present, no seasonal distinction in surface type (e.g. extent of snow cover) is made.

5.4. *Incorporation of stability*

Along with a distinction based on surface roughness, the wind modification is also defined in terms of stability, which is simply represented in terms of unstable (day) or stable (night) atmospheric conditions. Determining when to invoke a switch between these stabilities is complicated by the multi-dependent nature of the transitions between daytime and night-time boundary layers. Length of unstable and stable periods varies seasonally with solar insolation and is a function of such features as landuse type and moisture content of the surface and the adjacent air. The rate of convective boundary layer development is dependent on the strength of the previous nocturnal inversion (e.g. strong, moist inversions take longer to erode than those characterized as weak and dry). An additional consideration in the determination of a change between stable and unstable boundary layers is the fact that although conditions may be evolving in the lower levels of the boundary layer (e.g. generation of a convective boundary layer due to surface heating), the upper levels will retain previous boundary layer characteristics until the formative boundary layer is fully established.

In a study of inversions in rural areas, Takle (1983) observed that during the spring and winter months inversions began to develop near sunset and were sustained for a period just exceeding that of the sunset-to-sunrise time. Summer and fall inversions, on the other hand, were noted to begin prior to sunset and last 20–30% longer than the sunset-to-sunrise time. Godowitch and Ching (1980) analyzed the formation and growth of nocturnal inversion layers in both rural and urban environments during the months of July and August and indicate that in 95% of the cases studied a surface-based, rural inversion layer was initiated before sunset, with the majority of inversions forming within an hour prior to sunset. In contrast, over the urban environment an elevated inversion layer was established an average of $2\frac{1}{2}$ h after sunset. Investigation of O' Neill boundary layer data indicates a reversal in the sign of the heat flux (commonly an indicator of boundary layer change) approximately 1 h after sunrise and again about $1\frac{1}{2}$ h before sunset (Carson, 1973).

In light of the complexity of incorporating other measures of identifying transition times, sunrise and sunset times are used to provide the basis for determining when to employ the night-time adjustment and when to employ the daytime adjustment. The model computes trajectory endpoints at 1-h intervals to allow for greater trajectory resolution during the relatively short lengths of time associated with the individual CAPTEX releases. Given a 1-h time step (note that a particular adjustment of the wind must apply for the whole time step), the morning transition is made by checking the current time of the trajectory against the sunrise time for that location and the daytime adjustment is assumed if the sun has been up at least 2 h. As for the night-time transition, the current trajectory time is checked against the sunset time at that location and the night modification is used if the sun is setting or has already set.

6. RESULTS

6.1. *Comparison with CAPTEX observations*

To determine the response of the model to the new wind parameterization, trajectories are compared with observations from the Cross-Appalachian Tracer Experiment (Ferber *et al.*, 1986). This comparison provides an initial qualitative look at the nature of the trajectories produced under the modified formulation.

The CAPTEX releases selected for comparison are the two Sudbury releases, occurring on 26 and 29 October and the 18 September and 14 October releases from Dayton, Ohio. Trajectories are initiated hourly for each simulation, beginning at the time of tracer release and continuing through the respective sampling period. Although the duration of each release is 3 h, trajectories in the modified simulations are initiated for two additional hours as a means of further indicating the model-computed plume spread (i.e. six trajectories per modified model run are computed). At any given time the plume spread is approximated by the spatial distribution of trajectory endpoints. Trajectories are based on the objectively-analyzed surface pressure field of the time period in question. Results of the CAPTEX runs are shown in Figs 1–4. Each pair of figures represents the modified and original trajectory sets corresponding to a particular CAPTEX release.

Inspection of Figs 1(a) and 1(b), which show the relationship between the modified and original sets of trajectories and the observed concentration field for the 18 September release, reveals that the original trajectories are south of the observed plume area while the modified trajectory set closely simulates the direction of observed flow. To obtain a more definitive evaluation of plume/trajectory relationships, trajectory endpoints and locations of observed concentrations are examined at specified times during the sampling period. This analysis indicates that while south of the plume domain, the distance covered by the original trajectories relates to that expressed by the observation network. In contrast, comparison involving modified trajectory endpoints shows that by 14 h after the initial release the length of the trajectory set as a whole is roughly 750 km short of the observed extent of the plume. Also, model output reveals that the modified trajectories are ending prematurely in the vicinity of Lake Erie, indicating a problem with the self-consistent velocity field calculations when the trajectory encounters a change in surface type (from one CMC grid square to another). Essentially, the problem is one of the guess trajectory endpoints switching back-and-forth between 'rough' and

'smooth' grid squares during the trajectory iteration scheme.

Model results for the 14 October Dayton release are presented in Figs 2(a) and 2(b). Observations show the plume to follow a narrow, easterly path across Pennsylvania. As is evident, modified trajectories start in the general direction traveled by the plume, but later loop and take a northerly turn. The original trajectory set remains to the south of the observed concentration field. Plots of trajectory endpoints and stations of observed tracer concentration approximately 12 h after the initial release reveal that neither set of trajectories extends as far as observations indicate the plume has traveled. This lag suggests a simulation based on a slightly different wind field, which partially explains why the trajectory flow patterns differ from that exhibited by the tracer.

Trajectories of the tracer release from Sudbury on 26 October are shown in Figs 3(a) and 3(b). This release occurred in northwesterly flow immediately following

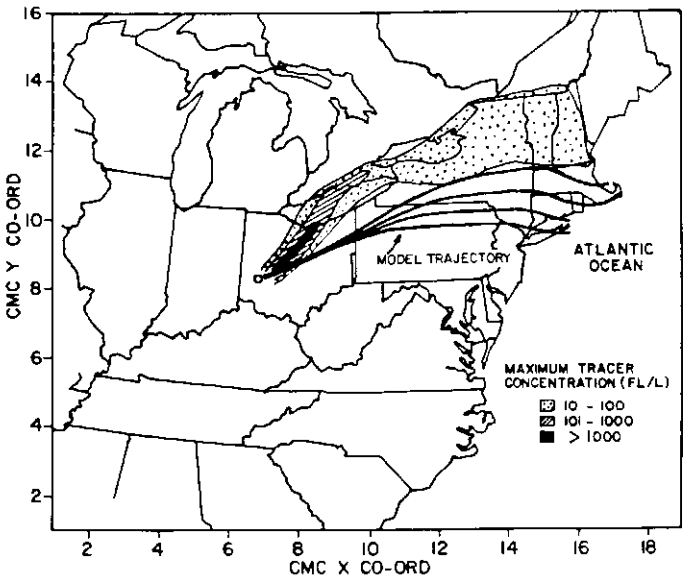

Fig. 1(a). Original model trajectories corresponding to the CAPTEX release from Dayton, Ohio on 18 September, 1700 GMT. Contours outline maximum observed concentrations of the released perfluorocarbon tracer (C_7F_{14}) during the sampling period (after Ferber *et al.*, 1986). Coordinate axes are labeled in terms of the Canadian Meteorological Center (CMC) grid.

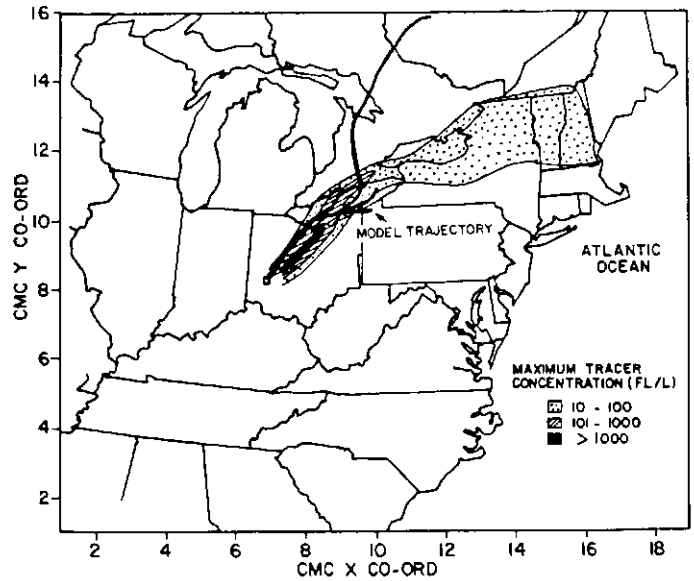

Fig. 1(b). Same as Fig. 1a, except for modified model trajectories.

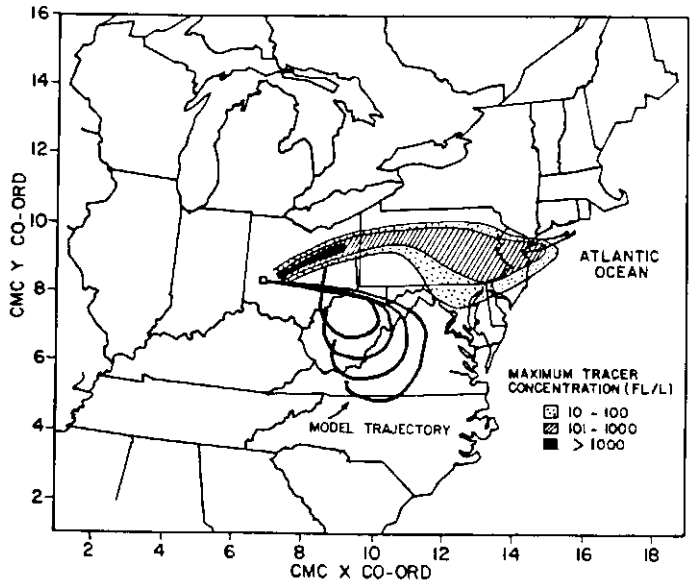

Fig. 2(a). Same as Fig. 1a, except the release from Dayton on 14 October, 1600 GMT.

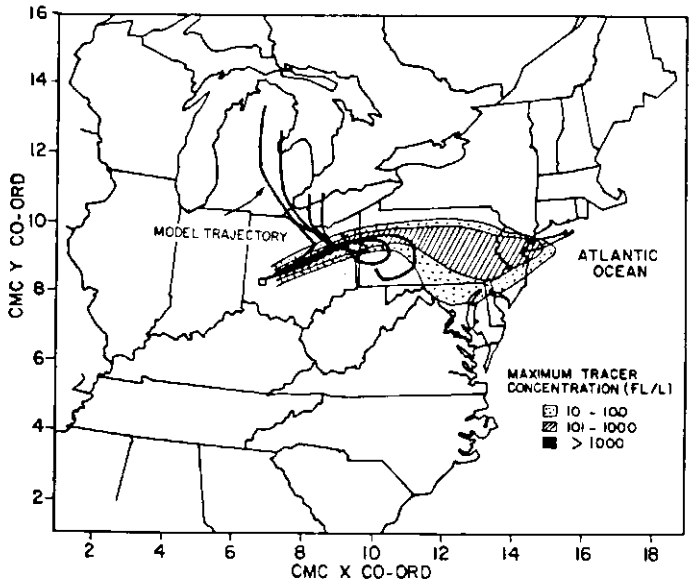

Fig. 2(b). Same as Fig. 2a, except for modified model trajectories.

passage of a cold front (Ferber *et al.*, 1986). As indicated, original trajectories exhibit a southerly path, remaining clear of the observed plume domain, while the modified trajectory set takes a southeasterly path. As with previous releases, modified trajectories tend toward the direction of observed concentration, but fall short in terms of total distance traveled.

Observations from the 29 October Sudbury release, presented in Figs 4(a) and 4(b), indicate a southerly direction of the plume, with maximum concentrations occurring in western New York and central Pennsylvania. This release also occurred after passage of a cold front (Ferber *et al.*, 1986). Modified trajectories take a southeasterly track, spreading predominantly over upstate New York, while the original trajectories demonstrate definite anti-cyclonic movement in the area west of the observed plume domain. This circulation relates to the high pressure center that was moving in eastward behind the front (Ferber *et al.*, 1986). Plots of trajectory endpoints and stations of observed tracer concentration indicate that the original trajectories extend roughly the same distance southward as the plume, while the modified trajectory set is approximately 150 km short of the observed

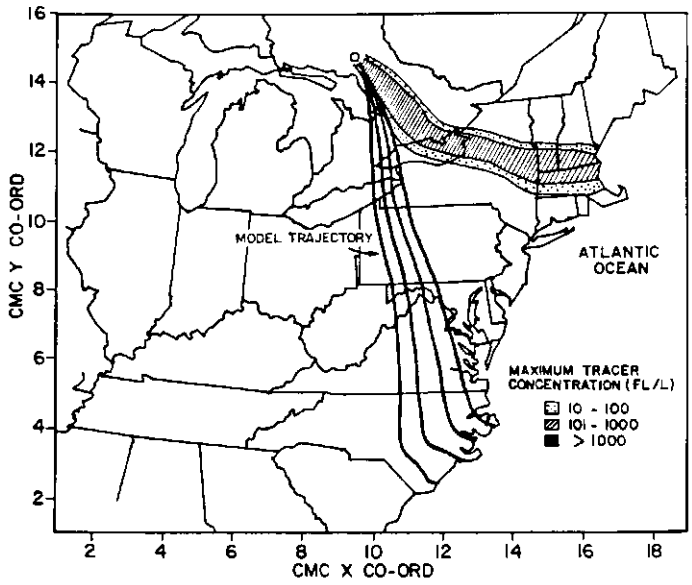

Fig. 3(a). Same as Fig. 1a, except the release from Sudbury on 26 October, 0400 GMT.

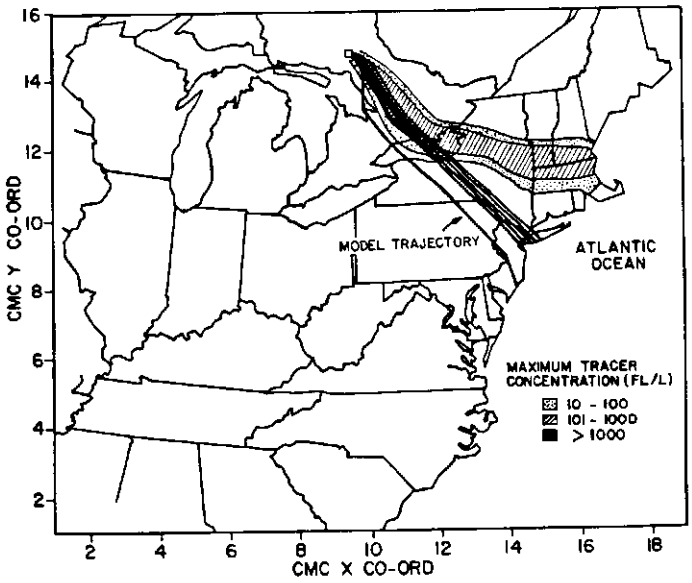

Fig. 3(b). Same as Fig. 3a, except for modified model trajectories.

distance traveled (at nearly 1 day after the initial release).

7. CONCLUSIONS

Parameterization of mean boundary layer flow in terms of surface geostrophic flow is developed and applied to a Lagrangian trajectory model. The wind modification in effect reduces the wind speed and backs the wind direction relative to surface geostrophic flow. To qualitatively assess whether or not the modified wind formulation enhances the predictive capability of the model, modified and original sets of trajectories are produced and compared with observations made during CAPTEX 83. Four of the seven tracer releases are used for comparison. While both techniques exhibit limitations in this particular application (i.e. short term), results indicate that the modified trajectories more closely identify the plume domain near the source (as depicted by the observation network), but lag the observed flow in terms of distance traveled.

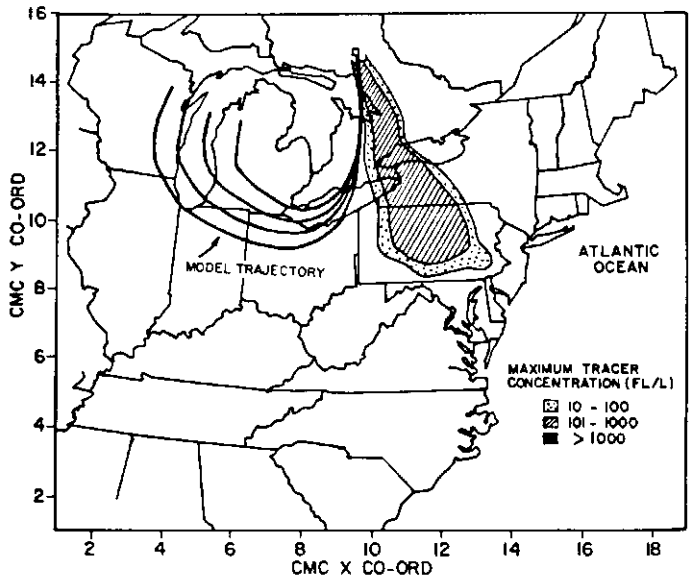

Fig. 4(a). Same as Fig. 1a, except the release from Sudbury on 29 October, 0600 GMT.

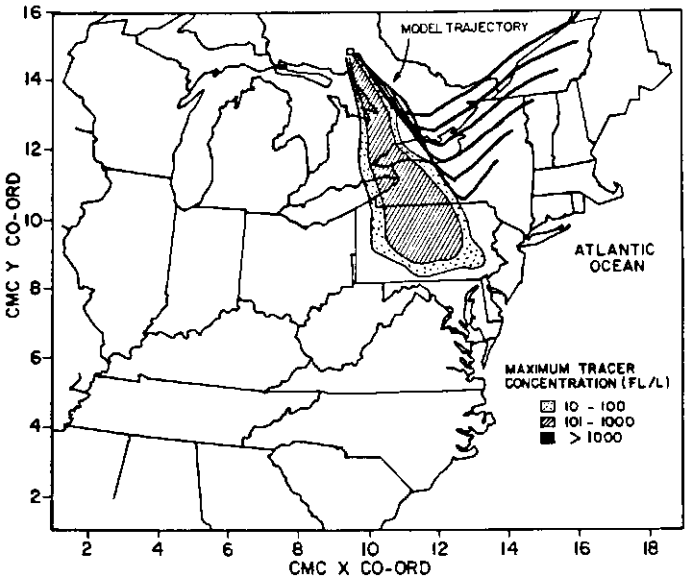

Fig. 4(b). Same as Fig. 4a, except for modified model trajectories.

Acknowledgements—The authors acknowledge the personnel of the Air Resources Branch of the Ontario Ministry of Environment who provided valuable assistance with the design and implementation of this project. Dr P. K. Misra, Dr Barbara Ley and Dr Gloria Ellenton are especially thanked for their insight and suggestions. The authors also extend thanks to Don Rhee and Sonny Wong, whose computer support and assistance were greatly appreciated. The landuse data were kindly supplied by Dr Chris Walcek of the National Center for Atmospheric Research.

This work was partly carried out at the Air Resources Branch, Toronto, Ontario.

REFERENCES

Anthes R. A., Seaman N. L. and Warner T. T. (1980) Comparisons of numerical simulations of the planetary boundary layer by a mixed-layer and a multi-level model. *Mon. Wea. Rev.* **108**, 365–376.

Arya S. P. S. (1975) Geostrophic drag and heat transfer relations for the atmospheric boundary layer. *Q. Jl R. met. Soc.* **101**, 147 161.

Carson D. (1973) The development of a dry inversion-capped convectively unstable boundary layer. *Q. Jl R. met. Soc.* **99**, 450–467.

Clarke R. H. (1970) Observational studies in the atmospheric boundary layer. *Q. Jl R. met. Soc.* **96**, 91–114.
Clarke R. H. and Brook R. R. (1979) The Koorin experiment: atmospheric boundary layer data over tropical savannah land. Department of Science, Canberra, Australia.
Clarke R. H., Dyer A. J., Brook R. R., Reid D. G. and Troup A. J. (1971) The Wangara experiment: boundary layer data. Tech. Paper **19**, CSIRO, Div. Met. Phys. Aspendale, Australia, 362.
Ellenton G., Ley B. and Misra P. K. (1985) A trajectory puff model of sulfur transport for eastern North America. *Atmospheric Environment* **19**, 727–738.
Ferber G. J., Heffter J. L., Draxler R. R., Lagomarsino R. J., Thomas F. L., Dietz R. N. and Benkovitz C. M. (1986) Cross-Appalachian Tracer Experiment (CAPTEX 83). Final Report, NOAA Technical Memorandum ERL ARL-142, Air Resources Laboratory, Silver Spring, MD.
Fisher B. E. A. (1984) The long-range transport of air pollutants—some thoughts on the state of modelling. *Atmospheric Environment* **18**, 553–562.
Garratt J. R., Wyngaard, J. C. and Francey, R. J. (1982) Winds in the atmospheric boundary layer—prediction and observation. *J. atmos. Sci.* **39**, 1307–1316.
Gillani N. V. (1983) Transport processes. The Acidic Deposition Phenomenon and Its Effects, Critical Assessment Review Papers, Vol. 1, Atmospheric Sciences, Chap. A-3, EPA-600/8-83-016AF.
Godowitch J. and Ching J. (1980) Formation and growth of the nocturnal inversion layer at an urban and rural location. Reprint from the Second Joint Conference on Applications of Air Pollution Meteorology and Second Conference on Industrial Meteorology, New Orleans, LA.
Haltiner G. and Martin F. (1957) *Dynamical and Physical Meteorology*. McGraw-Hill, New York.
Hess S. (1979) *Introduction to Theoretical Meteorology*. Krieger, New York.
Hidy G. M. (1984) Source–receptor relationships for acid deposition: pure and simple? A critical review. *J. Air Pollut. Control. Ass.* **34**, 518–531.
Hoxit L. R. (1974) Diurnal variations in planetary boundary layer winds over land. *Boundary-Layer Met.* **8**, 21–38.
Johnson W. R. (1983) Inter-regional exchanges of air pollution: model types and applications. *J. Air Pollut. Control. Ass.* **33**, 563–574.
Oke T. (1978) *Boundary Layer Climates*. Methuen, New York.
Rao S. T., Pleim J. and Czapski U. (1983) A comparative study of two trajectory models of long-range transport. *J. Air Pollut. Control. Ass.* **33**, 32–41.
Samson P. J. (1980) Trajectory analysis of summertime sulfate concentrations in the northeastern United States. *J. appl. Met.* **19**, 1382–1394.
Sheih C. M., Wesely, M. L. and Hicks, B. B. (1979) Estimated dry deposition velocities of sulfur over the eastern United States and surrounding regions. *Atmospheric Environment* **13**, 1361–1368.
Smith F. B. and Hunt R. D. (1978) Meteorological aspects of the transport of pollution over long distances. *Atmospheric Environment* **12**, 461–477.
Szepesi D. J. (1978) Transmission of sulfur dioxide on local, regional and continental scale. *Atmospheric Environment* **12**, 529–535.
Takle E. (1983) Climatology of superadiabatic conditions for a rural area. *J. Clim. appl. Met.* **22**, 1129–1131.
Thorpe A. J. and Guymer T. H. (1977) The nocturnal jet. *Q. Jl R. met. Soc.* **103**, 633–653.

APPENDIX

Regression datasets

Data sets used in the regressions of the mean boundary layer wind components on the magnitude of the surface geostrophic wind are listed below, with the input values identified. Here h is the boundary layer height (elevated inversion height for the night-time case); $\bar{U}$, $\bar{V}$ are the mean boundary layer wind components and G is the magnitude of the surface geostrophic wind.

Wangara day

Day	Time (GMT)	h (m)	$\bar{U}$ ($m s^{-1}$)	$\bar{V}$ ($m s^{-1}$)	G ($m s^{-1}$)
12	1200	850	7.24	0.89	10.10
12	1500	1400	6.34	1.12	9.23
13	1200	800	6.32	2.95	7.27
13	1500	900	6.70	1.92	8.18
33	1200	1000	2.80	0.24	5.70
33	1500	1200	3.33	0.59	6.28
34	1200	650	7.05	2.29	8.66
34	1500	1500	7.67	1.08	10.16

Koorin day

Day	Time (GMT)	h (m)	$\bar{U}$ ($m s^{-1}$)	$\bar{V}$ ($m s^{-1}$)	G ($m s^{-1}$)
6	1200	950	3.72	3.01	11.33
9	1200	1000	5.25	0.83	12.52
14	1200	900	3.27	2.64	9.07
15	1200	1400	4.08	2.65	7.92
17	1200	800	1.41	3.50	6.65
17	1500	1700	0.32	3.65	6.08
20	1500	2200	1.54	4.02	9.23
27	1500	1800	5.44	3.53	11.27
29	1200	1600	6.82	1.57	13.44
30	1200	1700	6.00	0.21	15.10

Wangara night

Day	Time (GMT)	h (m)	$\bar{U}$ ($m s^{-1}$)	$\bar{V}$ ($m s^{-1}$)	G ($m s^{-1}$)
6	2100	850	4.22	3.67	6.07
7	2100	850	6.76	1.68	5.59
8	0300	1400	7.72	2.07	5.33
11	2100	950	10.07	2.14	10.43
12	0000	1300	8.78	0.61	9.86
12	2100	1600	8.49	2.28	8.78
13	0000	1600	10.09	1.06	8.88
13	2100	1300	10.29	3.34	6.63
14	0000	1100	10.96	1.54	6.83
14	0300	1100	7.34	0.90	6.77
16	0000	750	12.44	0.22	10.79
16	0300	1100	9.99	1.05	9.46
18	2100	1300	9.36	1.32	9.67
19	0000	1300	8.92	0.00	8.88
19	0300	1500	7.91	0.83	8.17
31	0000	1000	13.21	0.46	11.79
31	0300	700	11.55	0.20	11.01
31	2100	1400	8.36	1.18	6.29
32	0000	1300	8.41	4.47	6.10
32	0300	1000	7.69	0.54	5.34
33	0000	1100	6.08	1.52	5.94
33	0300	1000	4.08	0.87	5.88
33	2100	1000	8.14	2.03	6.29
34	0000	1200	10.09	0.00	7.50
34	2100	1500	11.47	0.80	10.10
39	0300	700	10.54	0.74	9.98
43	0000	1700	6.92	2.38	8.49
43	0300	1600	9.03	2.42	10.52

Koorin night

Day	Time (GMT)	h (m)	$\bar{U}$ ($m s^{-1}$)	$\bar{V}$ ($m s^{-1}$)	G ($m s^{-1}$)
1	2100	1700	4.39	4.10	7.87
7	2100	2000	7.67	3.91	12.82
10	2100	2000	4.01	3.49	8.86
16	2100	2200	3.21	4.11	8.54
17	2100	1900	3.93	1.43	8.32
20	2100	2200	4.09	4.24	9.67
21	0000	2100	4.38	4.23	7.44
24	2100	2000	2.28	3.80	6.24

Confidence intervals for regression coefficients

The following are 95% confidence intervals for the regression coefficients b and b', where:

$$\bar{U} = bG \qquad \bar{V} = b'G.$$

Confidence intervals are determined by the expression: $b + SEt_{(n-1;\alpha/2)}$, where b represents the particular regression coefficient, t is the student's t statistic with $(n-1)$ degrees of freedom and SE is the associated standard error.

Wangara day
b (0.64, 0.82)
b' (0.07, 0.26)

Koorin day
b (0.30, 0.47)
b' (0.08, 0.33)

Wangara night
b (1.00, 1.15)
b' (0.10, 0.22)

Koorin night
b (0.42, 0.57)
b' (0.29, 0.52).

The following are confidence intervals for the subset regression sets referred to in Table 1.

Wangara night
b (1.01, 1.23)
b' (0.07, 0.23)

Koorin night
b (0.42, 0.61)
b' (0.30, 0.55)

Koorin day
b (0.11, 0.53)
b' (0.08, 0.51).